JOURNAL OF MATERIALS SCIENCE 29 (1994) 2315–2320

Mechanical behaviour, percolation and damage of materials with viscous solid grain boundaries

M. C. DANG, B. BAUDELET
Génie Physique et Mécanique des Matériaux, Unité Associée au CNRS, Institut National Polytechnique de Grenoble, ENSPG, BP46, 38402 Saint Martin d'Hères, France

The mechanical behaviour, percolation and damage mechanism of a aluminium alloy with viscous solid grain boundaries (GBs) at 465 °C have been characterized in experiments performed in tension or compression in the strain rate range of 10^{-5}–10^{-2} s^{-1}. It was found that grain-boundary sliding (GBS) occurs as strain rates below 10^{-4} s^{-1}. It was shown that the viscous solid interphase migrates during the process of deformation. In the case of tension, it was squeezed out of GBs parallel with the tension axis into GBs perpendicular to the axis and vice versa in the case of compression. This local percolation is discussed in terms of the viscosity of the interphase, gradient of local stresses and percolation time. The viscosity of the solid interphase is estimated. It was also found that cavitation depends on the type of stress (tension or compression) and the strain rate. Cavity nucleation occurs at multiple points when GBS happens or along GB facets in the absence of GBS. Cavity growth takes place along GBs at high normal stresses and the cavity coalsescence leads to "saw-tooth" fracture.

1. Introduction

A viscous grain boundary (GB) may be observed when the chemical or structural nature of the phases in the GB is different from that of grains. These GBs can exist in metallic alloys [1 11], ceramics [12 25], metal-matrix composites [26–28], frozen soils [29-31], ice [32–34] and alkaline salts [35–38].

The mechanical behaviour of materials with viscous GBs has received considerable attention because an understanding of the rheological effects of interphases is technologically important for the industrial application of the materials. It was shown that the compressive creep strain rates were enhanced when the grains were surrounded by sufficient liquid [2, 3, 25]. It is suggested that the mechanisms of joint lubrication, diffusion, cavitation and percolation may occur during deformation [2, 3, 18, 25, 36]. In a recent study, we have shown that the constitutive law depends strongly on the nature (solid or liquid) of the viscous intergranular phase and on the strain rate [4].

Percolation or fluid flow was suggested as a mechanism of accommodation [39, 40]. The effect of percolation on deformation has recently been analysed by a number of investigators [2, 5, 18, 41]. It was found that the percolation of liquid interphases occurs rapidly [2, 5] and is an important accommodation mechanism [5, 18].

Most studies to date have been focused on cavity nucleation and growth in viscous (i.e. amorphous) GBs of some ceramics because of the importance of their premature failure observed at high temperatures [20 25]. In these ceramics, cavities are always observed to be formed entirely within viscous GBs. It has also been shown that for materials with viscous interphases the damage occurs more rapidly in tension than in compression under similar conditions because the cavitation is promoted by tensile stresses [13, 20]. Similar behaviour has also been observed in metallic materials with a liquid GB phase [5]. In these materials tensile loading leads to more rapid failure, whereas a compressive loading tends to delay the process of failure. In addition, the damage produces intergranular fracture of "ball-like" grain shapes [5].

The evolution of cavities at viscous GBs and cavity geometries have been examined by a number of authors [16, 18, 21, 42, 43]. A wide variety of cavity geometries and sizes was shown. The most commonly observed cavity shape is a triangular wedge located at a multiple junction [16, 18, 21]. Another category of small cavities consists of holes of an oblate morphology formed along two-grain interfaces [21]. These oblate holes are only detected at high local stresses. Conversely, crack-like and full-facet cavities were observed at high stress levels in another study [42]. Additionally, these crack-like cavities extend across a grain facet, starting from a multiple point and becoming stabilized in the form of facet-sized cavities after extending into the opposite multiple junction. Consequently, because of the differences noted above, the cavity nucleation site and cavity geometries have received considerable attention in our investigations.

In this work the mechanical behaviour, percolation and damage evolution of the same aluminium alloy as that used previously [5] were studied by tensile and compressive tests at a temperature just below the fusion temperature of the GB phase. Furthermore, a comparison is made between the behaviour of the alloy with viscous solid GBs and that with liquid GBs.

0022–2461

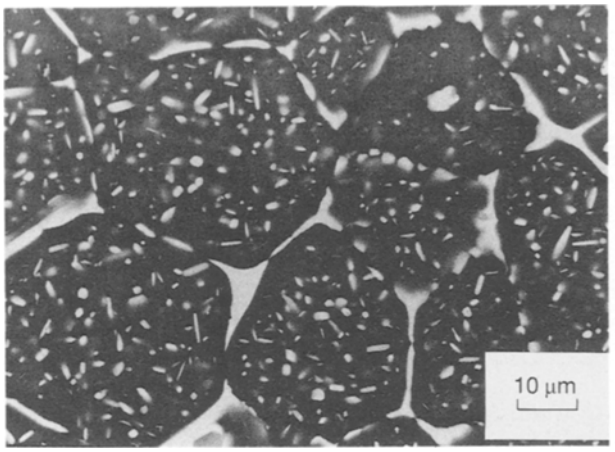

Figure 1 SEM micrograph of the microstructure of as-prepared Al-7000 alloy. The eutectic phase (white) is distributed along GBs as well as dispersed within grains.

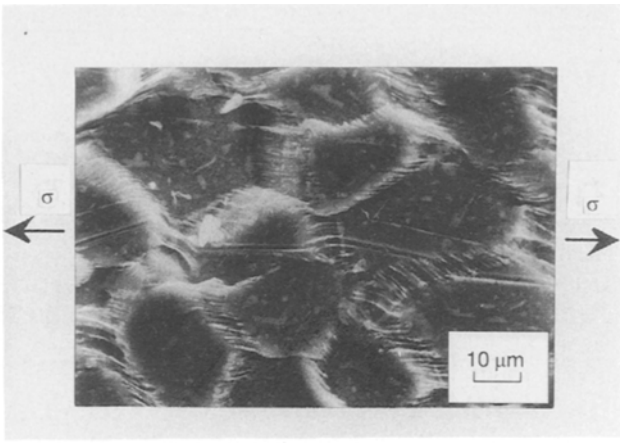

Figure 2 SEM micrograph showing grain-boundary sliding illustrated by the shift of scratches at grain boundaries and by surface relief of grains. The specimen was tested in tension at 465 °C, $\dot{\varepsilon} = 5 \times 10^{-5}\,s^{-1}$ for $\varepsilon = 0.25$.

2. Experimental procedure

The aluminium alloy used in this study is of the 7000 series prepared by Osprey. The microstructure of the material is composed of equiaxial grains of about 30 μm and a quaternary eutectic GB phase fusible at 477 °C (T_{GB}) [4]. This temperature is significantly lower than the melting temperature of the matrix material (630 °C). The alloy may be taken as a material with viscous solid GBs at 465 °C.

The microstructure of the material before testing is shown in Fig. 1. It is seen that the eutectic phase (white areas) exists in two forms: a semi-continuous network along GBs and small granular precipitates dispersed inside matrix grains. Previous investigations showed no significant evolution of the eutectic intergranular phase for relatively long annealing periods at temperatures lower than the eutectic fusion temperature [4]. Nevertheless, the eutectic intragranular phase of precipitates trapped inside the grains is more sensitive to thermal conditions because of the smaller sizes of the precipitates.

Mechanical tests were performed under inert gas at atmospheric pressure using a testing machine equipped with a furnace which ensures a quasi-constant temperature with an accuracy of $\pm 2°$. Tests were performed in compression or in tension at 465 °C with a strain rate ranging from 10^{-5} to $10^{-2}\,s^{-1}$. At the end of each test, the specimen was quenched into water to preserve the high-temperature microstructure. Nevertheless, some tensile tests reserved for the observation of pre-polished surfaces were terminated by cooling in the furnace under argon in order to preserve clean surfaces.

3. Results

3.1. Grain-boundary sliding

The existence of grain-boundary sliding (GBS) depends on the range of strain rates:

(i) At high strain rates ($\dot{\varepsilon} > 10^{-4}\,s^{-1}$), no visible GBS is observed. It is worth noting that the absence of GBS is related to low values of strain-rate sensitivity coefficient ($m \simeq 0.3$) and grain deformation comparable to the macroscopic deformation in compression [4].

(ii) At low strain rates ($\dot{\varepsilon} < 10^{-4}\,s^{-1}$), extensive GBS is observed. The GBS was evaluated by the shift of scratches at the grain boundaries and by the surface relief of grains (Fig. 2). The GBS is associated with high m values (~ 0.8) and quasi-equiaxial grains [4]. In this case the mechanical behaviour observed is comparable to that of a superplastic material.

In contrast, GBS is always observed at all strain rates when the intergranular phase is in the liquid state [5].

3.2. Percolation of viscous solid intergranular phase

The percolation of the GB phase is fluid flow of this phase along the GBs for certain distances. It is interesting to note that the long-distance percolation of interphase during compression observed in liquid GB materials [5] is absent in viscous solid GB materials under similar conditions. Micrographs of specimens tested in compression show the viscous solid phase squeezing out of boundaries nearly perpendicular to the compression axis and flowing into boundaries roughly parallel to the compression axis (Fig. 3a). This percolation is limited to distances comparable to the grain size (local percolation). The local percolation is also confirmed in tensile tests. In this case the viscous solid phase is expelled from GBs parallel to the tension axis and flows into those nearly perpendicular to the tension axis (Fig. 3b).

The occurrence of percolation depends on the magnitudes of t and σ at a given temperature, where t and σ are respectively the percolation time and applied stress in compression or in tension. In the (t, σ) space three zones can be recognized: no percolation, low percolation and high percolation. The zones with and without percolation can be separated by a straight line on a log–log plot (Fig. 4). In other words the time–stress behaviour observed seems to follow a hyperbolic relation:

$$t\sigma = K \tag{1}$$

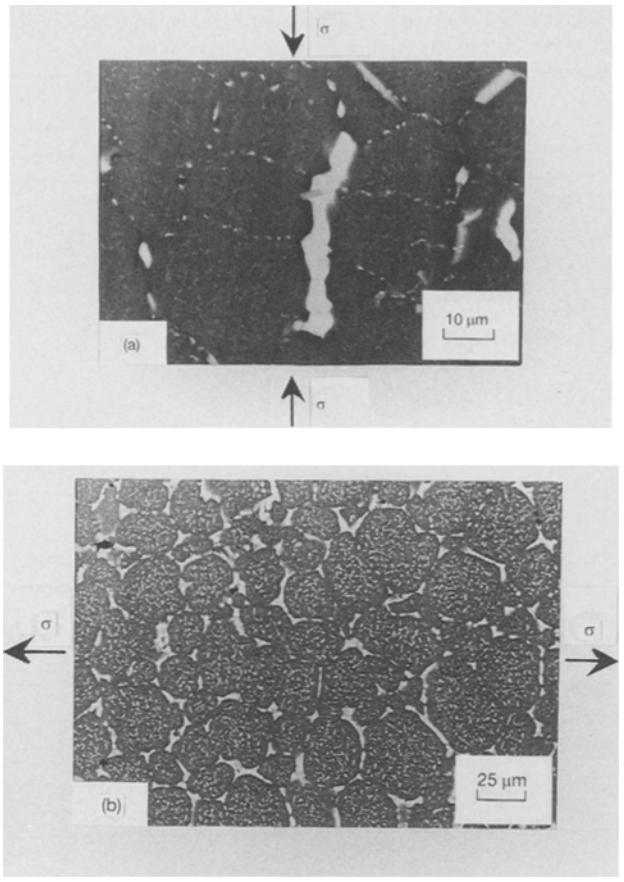

Figure 3 SEM micrographs showing local percolation. Interphase flowing into (a) GBs parallel to the axis of compression (test performed at 465 °C, $\dot{\varepsilon} = 6 \times 10^{-5} s^{-1}$ for $\varepsilon = 0.3$) and (b) GBs perpendicular to the axis of tension (test performed at 465 °C, $\dot{\varepsilon} = 5 \times 10^{-4} s^{-1}$ for $\varepsilon = 0.07$). Micrograph (b) exhibits less percolation because of shorter time. Small precipitates are formed in (b) due to slow cooling in furnace.

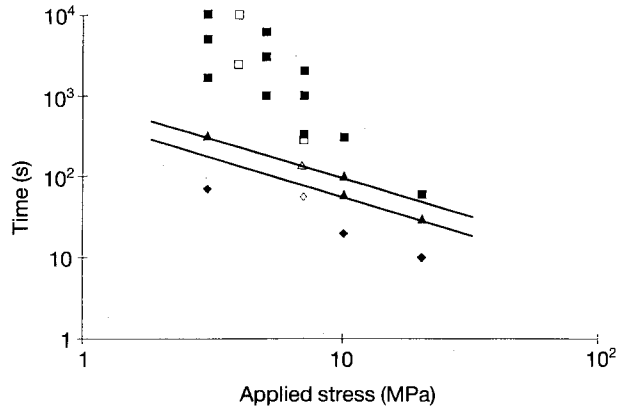

Figure 4 Dependence of the occurrence of percolation at 465 °C on the magnitudes of percolation time t and applied stress σ, shown on logarithmic scales: (■, ▲, ◆) in compression, (□, △ ◇) in tension. (□, ■) High percolation, (△, ▲) low percolation, (◇, ◆) no percolation.

where K is constant for a given temperature, approximately equal to 600–1000 MPa s at 465 °C.

3.3. Damage

In this material, cavitation appears in the GB phase and leads to ductile intergranular fracture. The damage behaviour also depends on the strain rate. In order

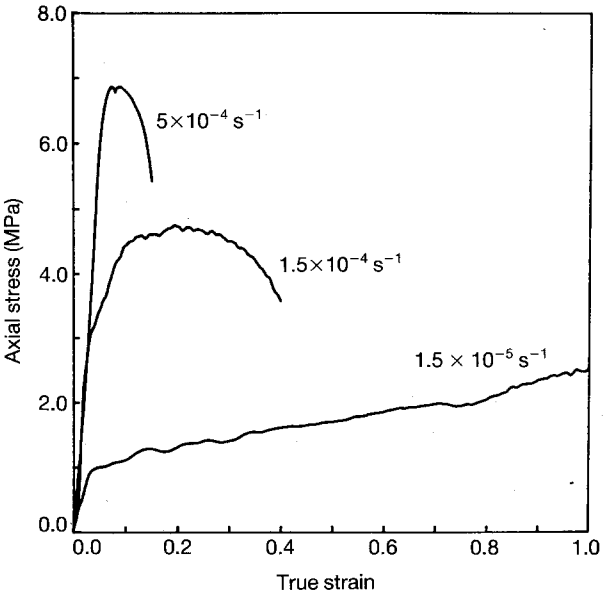

Figure 5 The effect of strain rate $\dot{\varepsilon}$ on the (σ–ε) behaviour in tension at 465 °C.

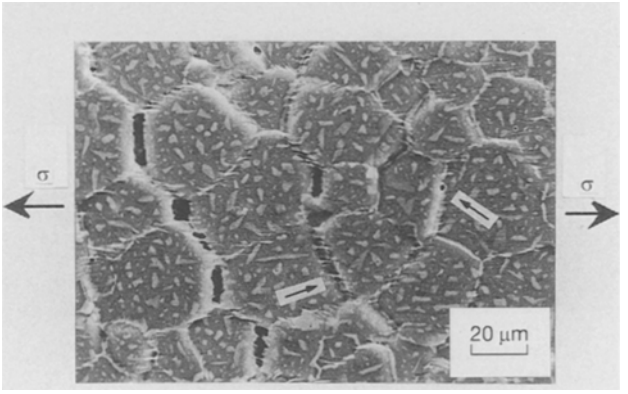

Figure 6 SEM micrograph of pre-polished specimen surface showing circular cavities nucleated at GB facets oriented roughly perpendicular to the tension axis (arrows) and coalescence along these GBs, after a test at a high strain rate $\dot{\varepsilon} = 5 \times 10^{-4} s^{-1}$, $T = 465$ °C and $\varepsilon = 0.15$.

to clarify cavitation mechanisms, a microstructural observation of specimens tested in tension was performed:

(i) At high strain rates ($\dot{\varepsilon} > 10^{-4} s^{-1}$, without GBS) the failure occurs at low strains and the cavitation influences the apparent constitutive law (Fig. 5). Cavities first nucleate at grain-boundary facets oriented perpendicular to the axis of tension instead of at multiple junctions. The cavities then grow and coalesce along the same GBs. The smallest cavities are circular holes and the bigger cavities (after growth and coalescence) have an oblate morphology. The intergranular coalescence occurs at inclined GBs lying between the GBs at which cavities are initiated (Fig. 6). Macroscopically, the resulting failure is of a "sawtooth" type. This phenomenon is observed both on the surface and in the bulk of specimens.

(ii) At low strain rates ($\dot{\varepsilon} < 10^{-4} s^{-1}$, with GBS), the material may be deformed to a very large strain

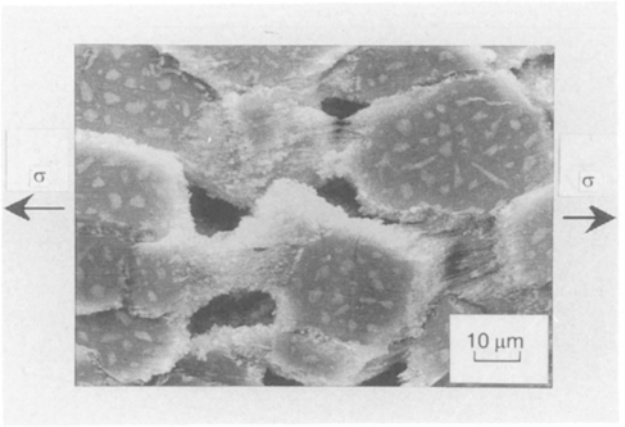

Figure 7 SEM micrograph of pre-polished specimen surface showing cavities nucleated at multiple points and coalescence along GBs oriented roughly perpendicular to the tension axis, after a test at a low strain rate $\dot{\varepsilon} = 1.5 \times 10^{-5}\,s^{-1}$, $T = 465\,°C$ and $\varepsilon = 0.62$.

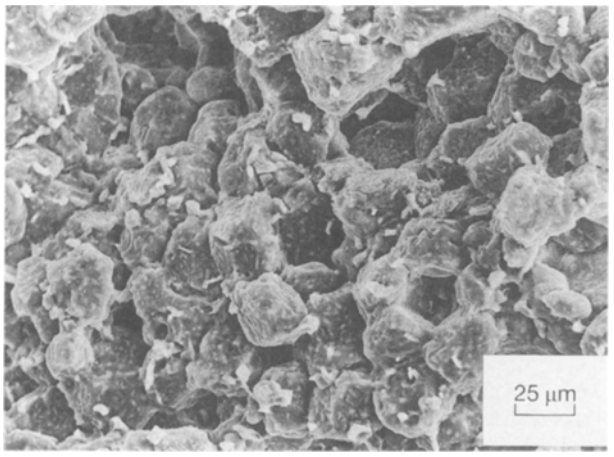

Figure 8 SEM micrograph of an intergranular fracture surface showing angular grain shapes after a tensile test at 465 °C, $\dot{\varepsilon} = 5 \times 10^{-4}\,s^{-1}$ for $\varepsilon = 0.15$.

without fracture (for example up to $\varepsilon = 1$, for $\dot{\varepsilon} = 1.5 \times 10^{-5}\,s^{-1}$) (Fig. 5). In this case the damage mechanism is different from that observed when strain rates are high. Equiaxed cavities apparently nucleate at multiple points and propagate into GB facets perpendicular to the tension axis. After growth and coalescence the cavities become wedge-shaped (Fig. 7). No intergranular coalescence is found. This is also observed in microstructural examination of cross-sections of specimens. The above damage mechanism has also been observed when the intergranular phase is liquid, when GBS appears at all strain rates [5].

The damage of material with viscous solid GBs always produces intergranular fracture of angular grain shapes (Fig. 8) whereas that of more rounded grain shapes has been observed under similar conditions when the GBs are liquid [5].

The final stage of damage evolution (no cavitation, nucleation and growth along GBs, coalescence and failure) depends on the type of stress (tension or compression), the state of interphases (solid or liquid) and the range of strain rates (Table I). It is interesting to compare the results obtained from tensile and compressive tests under similar conditions. In compression, the evolution of damage is slower than that

TABLE I Final stages of damage observed in tensile and compressive tests for materials with solid or liquid GBs

		Final stage of damage	
Type of stress	Strain rate	Solid GBs	Liquid GBs
Tension	High	1. Failure	5. Failure
	Low	2. Growth[a]	6. Failure
Compression	High	3. Growth[b]	7. Failure
	Low	4. No cavitation[b]	8. Growth[b]

[a]Tensile tests up to 100% deformation.
[b]Compressive tests up to 60% deformation.

in tension: intergranular rupture takes place at 15% deformation in tension (Fig. 5), whereas a specimen can be deformed up to 60% without coalescence and failure in compression in the same range of strain rates [4]. We note also that the damage process occurs more rapidly when the GB phase is liquid (Table I).

4. Discussion

4.1. Grain-boundary sliding and local tensile stress at the grain boundaries

When a remote stress is applied, GBS occurs on inclined boundaries across which large shear stresses exist as shown in Fig. 2. The GBS happens with a relatively short relaxation time and can generate stress concentrations on adjacent boundaries; the physics describing it has been well analysed [2, 12, 14, 21, 22, 24, 44, 45]. For usual materials, the stress levels induced by GBS are considerably higher than the applied stresses, especially at multiple points [44, 45]. In the case when a viscous solid phase is present along GBs, the stresses induced by GBS at multiple junctions are probably relaxed. When the GB phase is liquid these stresses will be relaxed and become negligible in comparison with the applied stress. As a result the distributions of local tensile stresses, σ_{GB}, on GBs parallel and perpendicular to the stress axis are as presented in Fig. 9. The σ_{GB} level equals approximately the applied stresses, σ_T for tension or $-\sigma_C$ for compression, at GBs perpendicular to the corresponding axis of the applied stress.

By the same arguments we may estimate the magnitude of the gradients of the local stresses, $\Delta\sigma$, between two boundaries parallel and perpendicular to the stress axis. At a given temperature, this gradient of the local stresses is approximately equal to the applied stress.

4.2. Percolation driven by gradient of stress between two boundaries

A gradient of stress includes the percolation of viscous solid interphase and confirms the experimental results observed above (Figs 3 and 4). The kinetics of flow of the viscous phase out of those GBs experiencing compressive forces can be considered according to a simple model for the flow of a Newtonian liquid of viscosity η and original thickness h_0 from between two flat plates of radius r pressed together at constant

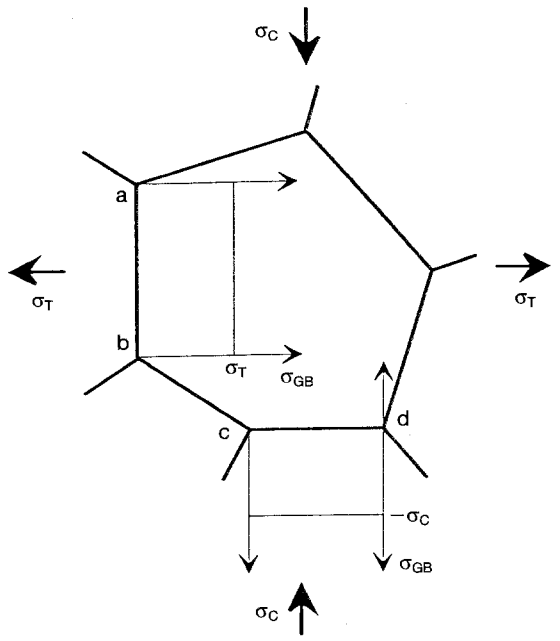

Figure 9 Schematic diagram and formulation of local stress distribution, σ_{GB}, along GBs (a–b, c–d) parallel and perpendicular to the stress axis. In tension $\sigma_{GB}^{ab} = \sigma_T$, $\sigma_{GB}^{cd} = 0$ and $\Delta\sigma = \sigma_T$; in compression $\sigma_{GB}^{ab} = 0$, $\sigma_{GB}^{cd} = -\sigma_c$ and $\Delta\sigma = \sigma_c$, where $\Delta\sigma$ is the gradient of local stresses between two GBs a–b and c–d.

stress σ [2]:

$$t\sigma = \frac{3}{4}\eta r^2 \frac{1}{h_0^2}\left[\left(\frac{h_0}{h_{(t)}}\right)^2 - 1\right] = K \qquad (2)$$

Here h_t is the thickness of liquid film which decreases with time t. Equation 2 describes a hyperbolic relation between t and σ, which agrees with the experimental results shown in Fig. 4. This relation can be used to determine the viscosity value of the interphase at 465 °C. At this temperature, the parameters appearing in Equation 2 are $2r = 30$ μm (grain size), $h_0 = 1$ μm (initial thickness of interphase), $h_0/h_{(t)} = 10$–50 (as determined from the micrographs as shown in Fig. 3) and K is as estimated above in section 3.2. The viscosity of the viscous solid phase, η_s, is calculated according to Equation 2 to be 10^3–10^4 N s m^{-2}. These values lie between those for liquid metals, $\eta_L \simeq 10^{-3}$ N s m^{-2} [46], and for the glass at GBs in ceramics, $\eta = 10^6$ N s m^{-2} [41]. The fact that $\eta_s/\eta_L = 10^6$–10^7 and $t \propto \eta$ (Equation 2) allows us to understand why the percolation of liquid phase occurs very rapidly and over long distances in compression [2, 5], while the percolation of viscous solid phase is limited to distances comparable to the grain size (for the limited time of the mechanical tests), as observed in this study.

4.3. Damage caused by local tensile stresses at grain boundaries

The damage may appear at GBs with the highest normal tensile stress (a–b in Fig. 9). The cavity formation at these boundaries depends on the σ_{GB} levels as discussed below.

At high strain rates (without GBS), the uniform high value of σ_{GB} along a–b in tension provokes the nucleation of cavities at GB facets (Fig. 6) and consequently the failure at small strains (Fig. 5, labelled 1 in Table I). In compression, the corresponding value of σ_{GB} along a–b is null and tends not to provoke cavity nucleation. However, the heterogeneous deformation associated with compressive tests may produce a certain σ_{GB} [5, 47]. In this case σ_{GB} depends on the applied stress σ_C and may promote a weak cavitation, which is in good agreement with the present results (labelled 3 in Table I).

At low strain rates (with GBS) there are at least two hypotheses that may interpret the preferential nucleation of cavities at multiple points: one is associated with the high stresses induced by GBS at multiple junctions as discussed above (section 4.1); the other is related to the difficulty in maintaining the cohesion of material at solid contacts between grains when GBS occurs. Although the former has been suggested by a number of investigators [21, 43, 45] and the present authors [5], we tend to use the latter as an alternative concept. When the viscosity of the solid interphase is low at temperatures just below T_{GB} (section 4.2) the first hypothesis becomes less reasonable, with the extreme case of being untenable when the interphase is liquid. The second hypothesis is associated with a number of theoretical problems, in particular solution–precipitation processes [19]. These processes appear to be necessary in order for solid contacts between grains to be sustained during deformation. Details of this problem are currently being investigated. Once nucleated, cavities grow along GBs with the highest normal tensile stress. As shown in Figs 7 and 9, these GBs are oriented roughly perpendicular to the axis of tension. Because of the small σ_T values at low strain rates, the σ_{GB} produced is not large enough to cause failure (Fig. 5, labelled 2 in Table I). For compressive tests, the value of σ_{GB} along a–b in Fig. 9 is nearly null and as a result no cavitation is generated (labelled 4 in Table I). In this case, the local tensile stresses induced by heterogeneous deformation (related to compressive tests) are assumed to be too small to provoke cavity nucleation.

5. Conclusions

1. The mechanical behaviour, percolation and damage evolution in an aluminium alloy with viscous solid intergranular phase have been shown.

2. The local percolation, or the flow of viscous solid interphase into GBs perpendicular to the tension axis or parallel to the compression axis, depends on time t and applied stress σ according to the hyperbolic relation $\sigma t = K$, where K is constant at a given temperature.

3. The viscosity of the GB phase in the alloy at 465 °C has been evaluated to be 10^3–10^4 N s m^{-2}, which is significantly higher than that of liquid metals (about 10^{-3} N s m^{-2}). As a consequence, the percolation of viscous solid interphase is limited to distances comparable to the grain size.

4. The percolation process is driven by the gradient of local stresses, $\Delta\sigma$, due to the applied stresses.

5. The cavitation is induced by tensile local stresses, σ_{GB}, acting on GBs and it occurs at GBs perpendicular to the tension axis or parallel to the compression axis.

6. The cavitation mechanism depends on the strain rate. At high strain rates (without GBS) cavities nucleate and grow at GB facets. On the other hand, they occur at multiple junctions at low strain rates (with GBS).

7. The damage produces intergranular fractures of angular grain shapes.

Acknowledgements

The authors would like to thank Pechiney (Voreppe) for the supply of materials and Drs F. Bordeaux, D. Ferton and Y. Liu for fruitful discussions.

References

1. B. L. VAANDRAGER and G. M. PHARR, *Scripta Metall.* **18** (1984) 1337.
2. *Idem, Acta Metall.* **37** (1989) 1057.
3. G. M. PHARR, P. S. GODAVARTI and B. L. VAANDRAGER, *J. Mater. Sci.* **24** (1989) 784.
4. B. BAUDELET, M. C. DANG and F. BORDEAUX, *Scripta Metall. Mater.* **26** (1992) 573.
5. F. BORDEAUX, M. C. DANG and B. BAUDELET, *J. Mater. Sci.* in press.
6. M. C. ROTH, G. C. WEATHERLY and W. A. MILLER, *Acta Metall.* **28** (1980) 841.
7. D. D. PETROVIC, G. C. WEATHERLY and W. A. MILLER, *ibid.* **36** (1988) 2249.
8. A. WOLFENDEN and W. H. ROBINSON, *ibid.* **25** (1977) 823.
9. D. WEBSTER, *Metall. Trans.* **A18** (1987) 2181.
10. M. F. WEILL, Ph D Thesis, Université Pierre et Marie Curie Paris VI (1979).
11. Y. S. NECHAEV, *Coll. Physique C1* **51** (Suppl. to No. 1) (1990) 287.
12. K. H. CHAN, J. LANKFORD and R. A. PAGE, *Acta Metall.* **32** (1984) 1907.
13. P. K. TALTY and R. A. DIRKS, *J. Mater. Sci.* **13** (1978) 580.
14. A. G. EVANS and A. RANA, *Acta Metall.* **28** (1980) 129.
15. M. D. THOULESS and A. G. EVANS, *ibid.* **34** (1986) 23.
16. F. F. LANGE, B. I. DAVIS and D. R. CLARKE, *J. Mater. Sci.* **15** (1980) 601.
17. D. R. CLARKE, *ibid.* **20** (1985) 1321.
18. R. M. ARONS and J. K. TIEN, *ibid.* **15** (1980) 2046.
19. R. RAJ and C. K. CHYUNG, *Acta Metall.* **29** (1981) 159.
20. R. MORRELL and K. H. G. ASHBEE, *J. Mater. Sci.* **8** (1973) 1253.
21. J. E. MARION, A. G. EVANS, M. D. DRORY and D. R. CLARKE, *Acta Metall.* **31** (1983) 1445.
22. R. A. PAGE, D. J. LANKFORD and S. SPOONER, *ibid.* **32** (1984) 1275.
23. R. RAJ, *Coll. Physique* **51** (1990) C1-393.
24. R. L. TSAI and R. RAJ, *Acta Metall.* **30** (1982) 1043.
25. G. M. PHARR, in "Ashby Symposium: The Modelling of Material Behavior and its Relation to Design", edited by J. D. Embury and A. W. Thompson (TMS, London, 1990) p. 89.
26. T. G. NEIH and J. WADSWORTH, "High Strain Rate Superplasticity in Metal Matrix Ceramics", Internal Report (Lockheed, London, 1990).
27. O. D. SHERBY and J. WADSWORTH, *Progr. Mater. Sci.* **33** (1989) 169.
28. R. S. MISHRA and A. K. MUKHERJEE, *Scripta Metall.* **25** (1991) 271.
29. G. M. PHARR and J. E. MERWIN, *Cold Reg. Sci. Technol.* **11** (1985) 205.
30. G. M. PHARR and P. S. GODAVARTI, *ibid.* **14** (1987) 273.
31. M. S. NIXON and G. M. PHARR, *J. Ener. Resour. Technol.* **106** (1984) 344.
32. P. DUVAL, in Proceeding of Conference on Isotopes and Impurities in Snow and Ice, Grenoble, August 1975 Publication No. 118 (IAHS, Grenoble, 1977) p. 29.
33. P. S. GODAVARTI and G. M. PHARR, *J. Ener. Resour. Technol.* **107** (1985) 173.
34. L. LLIBOUTRY, *J. Glaciology* **10** (1971) 15.
35. T. BAYKARA and G. M. PHARR, *Acta Metall. Mater.* **39** (1991) 1141.
36. G. M. PHARR and M. F. ASHBY, *Acta Metall.* **31** (1983) 129.
37. R. SHEIKH and G. M. PHARR, *Scripta Metall.* **18** (1984) 837.
38. *Idem. Acta Metall.* **33** (1985) 231.
39. O. REYNOLDS, *Phil. Mag.* **20** (1885) 469.
40. F. C. FRANK, *Rev. Geophys.* **3** (1965) 485.
41. S. M. WIEDERHORN, B. J. HOCKEY, R. F. KRAUSE Jr and K. JAKUS, *J. Mater. Sci.* **21** (1986) 810.
42. J. R. PORTER, W. BLUMENTHAL and A. G. EVANS, *Acta Metall.* **29** (1981) 1899.
43. M. D. THOULESS and A. G. EVANS, *J. Amer. Ceram. Soc.* **67** (1984) 721.
44. J. CADEK, in "Creep in Metallic Materials" (Elsevier, Amsterdam, 1988) p. 279.
45. A. G. EVANS, J. R. RICE and J. P. HIRTH, *J. Amer. Ceram. Soc.* **63** (1980) 368.
46. G. F. CARTER, in "Metals Handbook: Mechanical, Physical and Chemical Properties of Metals", edited by H. E. Boyer and T. L. Gall (American Society for Metals, Ohio, 1985) p. 2–19.
47. R. W. EVANS and B. WILSHIRE, in "Creep of Metals and Alloys" edited by D. McLean (Institute of Metals, London, 1985) p. 51.

Received 22 June
and accepted 28 September 1993